Upper bound solutions for the shape factors of smooth rectangular footings on frictional materials

Ashraf S Osman[1]

Abstract

Limit analysis of smooth square and rectangular footings is presented in this paper. Three dimensions multi-block collapse mechanism with kinematically admissible velocity field is developed. The rigid blocks in this mechanism are truncated by conical surfaces. Rigorous upper bound solutions for the bearing capacity of the footings in frictional soils are obtained by assuming the normality rule. The numerical results of the shape factors are presented in the form of design charts for practical use in geotechnical engineering.

Keywords: Upper bound limit analysis, frictional material, footings

[1] Department of Engineering, Durham University, South Road, Durham DH1 3LE, UK.
Tel: +44 191 3342425 Email: ashraf.osman@durham.ac.uk

Introduction

The bearing capacities of square and rectangular footings on sand are traditionally estimated from the plane-strain solutions of strip footings (e.g. [1-9]) by applying empirical modifications to account for the finite length. Empirical shape factors to adjust strip footings solutions were proposed by Meyerhof [3] De Beer [10] Brinch Hansen [11] among the others.

For a rectangular footing bearing capacity equation takes the form:

$$p = N'_c c + N'_q q + \frac{1}{2}\gamma B N'_\gamma \tag{1}$$

where p is the limiting pressure on the footing, q is the surcharge, γ is the unit self-weight of the soil, c is the soil cohesion and N'_c, N'_q and N'_γ are bearing capacity factors related to the cohesion, the surcharge and the weight of the soil respectively. The bearing capacity factors N'_c, N'_q and N'_γ are related to the bearing capacity of strip footings via shape factors s_c, s_q and s_γ:

$$\begin{aligned} N'_c &= s_c N_c \\ N'_q &= s_q N_q \\ N'_\gamma &= s_\gamma N_\gamma \end{aligned} \tag{2}$$

where N_c, N_q and N_γ are the corresponding bearing capacity factors for a strip footing.

For a strip footing in a weightless cohesionless soil, the bearing capacity factor N_q can be given by [12]:

$$N_q = \frac{1+\sin\phi}{1-\sin\phi} e^{\pi \tan\phi} \quad (3)$$

where ϕ is the friction angle of the soil.

Caquot [13] has introduced the theorem of correspondence state, which made it possible to obtain a solution for cohesive-frictional soils by the transformation of a known solution for a purely frictional material and has shown that:

$$N_c = \frac{N_q - 1}{\tan\phi} \quad (4)$$

While equations 3 and 4 give exact solutions for N_c and N_q for strip footings on weightless soils, the exact solution for N_γ is indeterminate. There are several solutions for the bearing capacity factor N_γ in the literature (e.g.[2-8,10,14-18]). The differences among these solutions are often very substantial. Some of the common proposed expressions are listed in Table 1. Recently, Martin [8] used the method of characteristics and obtained numerical values for N_γ,which is claimed to be exact since it was shown that, through the refinement of the mesh of characteristics, it is possible to extend the stress field beyond the plastic volume and achieve coincidence of the stress and velocity calculations.

Commonly used empirical expressions for the shape factors s_q, s_γ and s_c are given in Table 2 where L is the length of the footing and B is the width.

It should be noted that superposition of the three components in Equation 1 is not theoretically correct unless the principal stress trajectories associated with partial solutions coincide. Smith

[13] has shown that for cohesionless soil, the superposition of the second and the third terms of Equation 1 can underestimate the bearing capacity factor by up to 25%. Detailed discussion on the superposition principle can be found in [19] and [20]. Nevertheless, the superposition approach has been widely used in engineering practice and has been adopted in several design codes (e.g. Eurocode 7 (EC7) [17] and the AASHTO LRFD Bridge Design Specifications [18]).

There are few analytical or numerical solutions for the shape factors of rectangular footings in frictional materials. Early rigorous solutions for shape factors for smooth footing were proposed by Shield and Drucker [21]. These solutions are based on the upper-bound limit analysis theorems. However, these solutions have been proposed only for frictionless soils for which the collapse mechanisms are not as complex as those for frictional soils. In frictional materials, the dilation and the requirement to satisfy the normality rule in limit analysis make it difficult to construct admissible velocity fields in three-dimensions. The complexity of the geometry of the three-dimensional mechanisms makes the upper bound calculations quite elaborate. Almost five decades had passed since before Michalowski [22] presents the first upper bound solutions for rectangular footings in frictional materials together with admissible three-dimensional velocity fields. Michalowski [22] has also proved that if the boundary stress (the surcharge) is perpendicular to the boundary of the collapse mechanism and the intermediate principal plastic strain rate is zero then the calculations of work dissipation rate on the velocity discontinuity surfaces and within the deformation regions of the soil can be replaced by a much simpler surface integral. This result in simple calculations for the bearing factor N_c' for rectangular footing as it can be obtained directly from N_q' using the linear transformation:

$$N_c' = \frac{N_q' - 1}{\tan \phi} \tag{5}$$

Equation 5 implies that the theorem of correspondence of Caquot (Equation 4) can be extended to rectangular footing under certain conditions.

Numerical techniques have been used recently to analyse rectangular footings. Michalowski and Dawson [23] used the finite difference method to study the collapse mechanisms of rectangular footings in frictional materials. Zhu and Michalowski [24] carried out finite element analysis to obtain shape factors for rectangular footings in frictional materials. Lyamin et al. [25] used Finite Element Limit Analysis (FELA) to derive solutions for rectangular footings in sand. In their formulation, linear stress (lower bound) and linear velocity (upper bound) triangular finite elements were used to discretise the soil mass. Every node in the FELA mesh is unique to a particular element so that statically admissible stress (LB) and kinematically admissible velocity discontinuities (UB) can occur along shared edges between adjacent elements. Finite element formulation with quadratic velocity fields was used by Antão et al. [26] to derive upper bound solutions for the shape factors. In the analytical and numerical solutions for rectangular footings cited above the footings are assumed to be rough and fully bonded to the soil underneath (although smooth footings were briefly discussed in [23], the reported results are limited to purely-cohesive soil case). Yang et al. [27] attempted to analyse smooth rectangular footings using a lower bound limit analysis finite element technique. Admitting the difficulty of implementing Mohr-Coulomb failure criterion in three dimensions, Yang et al. [27] used Drucker-Prager failure criterion instead, and the analysis was limited to footings on weightless cohesive soils without surcharge loads. Lower bound solutions for

smooth rectangular footings on Mohr-Coulomb soils were reported by Lyamin and Sloan [27], but they are limited to soils with small angles of friction $\phi \leq 20^{\circ}$.

Assuming a rectangular footing to be rough or fully-bonded to the soil could lead to an optimistic estimate for the bearing capacity. In strip footings in frictional materials, the soil-footing interface could have a significant impact on the bearing capacity. Gourvenec et al. [29] showed that the bearing capacity factor N_c for a smooth square footing on a purely cohesive soil is about 13% less than its value in a rough footing. Figure 1a compares that bearing capacity factor N_γ in a smooth strip footing to that of a rough strip footing. The values of N_γ are obtained from the method of characteristics using the ABC software of Marin [8]. This figure shows that N_γ in a smooth strip is lower than its value in a rough footing. Figure 1b plots the values of N_γ in a smooth strip footing normalised by the corresponding values in a rough strip footing. It can be shown that the bearing capacity factor N_γ in a smooth strip is about 50% of that of a rough strip footing when the friction angle $\phi = 40^{\circ}$. The influence of the footing roughness reduces at small friction angles. However, even at $\phi = 5^{\circ}$, N_γ in a smooth strip foundation is about 75% of that of a rough foundation. This paper presents an attempt to derive the shape factors for smooth rectangular footings in frictional materials analytically. Upper bound limit theorem together with an admissible three dimensions multi-block collapse mechanism is used to obtain the shape factors. In this paper, the soil mass is taken to be governed by the Mohr-Coulomb failure criterion. In order to obtain rigorous upper bound solutions, the soil is assumed to obey associative flow rule so that the dilation angle is taken to be equal to the friction angle ϕ.

Multi-Block Collapse Mechanism

Construction of the collapse mechanism

Figure 2 shows the multi-block collapse mechanism proposed for smooth rectangular footing. The faces of the rigid block are constructed from conical surfaces and tangential surfaces. All the conical surfaces have an apex angle of 2ϕ. The figure shows a plan view (Figure 2a) and views from the top and the bottom (Figure 2b and 2c). A projection of the mechanism in a vertical plane is shown in Figure 2d. The projection in a vertical plane resembles the well-known Hill mechanism [30] for plane-strain strip footings. However, the continuous deformation fan zone is replaced here by a series of rigid blocks. The proposed mechanism is different from the three-dimensional mechanism of rough footings [22] as the projection of the latter in a vertical plane resembles a Prandtl mechanism [31].

The multi-block mechanism is constructed in such a way that the direction of the velocity of each rigid block coincides with the axis of its respective cone. This is an essential condition to ensure that velocity vectors are inclined at an angle ϕ to the discontinuity surfaces separating the mechanism from the soil at rest and therefore, satisfy the normality requirement. The truncation of rigid blocks by conical surfaces could also lead to better upper bound solutions [22][32][33].

Figure 3 demonstrates the construction of a five-block flank of the mechanism. Each cone is the mirror image of the adjacent cone with respect to the plane that is normal to the discontinuity surface separating the adjacent rigid blocks (as illustrated in Figure 3b). Therefore, the ellipsoidal cross-section of each of the adjacent cones on the discontinuity surface becomes identical, and the kinematic admissibility of the mechanism is ensured. Once the cones are constructed, and their intersections with the discontinuity faces (the ellipsoidal

cross-section) are found, the tangential planes are then established. In Figure 4, an ellipsoidal cross-section along the discontinuity characterised by line IV is shown as an example together with the tangent line MK. In this figure, α_i and β_i are the angles defining the geometry of the projection of the mechanism on a vertical plane, and v_i refers to the kinematically admissible velocity of the rigid block *i*. v_{ij} refers to the velocity jump along the discontinuity between blocks i and j. The compatible velocities v_i and $v_{i,j}$ can be calculated from the hodograph shown at the bottom right corner of Figure 4. Further details of the calculations are given in Appendix A.

The rigid block mechanism is taken to have only one plane of symmetry with its normal coincides with the footing longitudinal direction and the parameters ζ_1 and ζ_2 defines the location of the apex of the first cone (A_1). The drive to have only one plane of symmetry comes from the early work of Shield & Drucker [21] and Michalowski [22] on square footings which have found that using two planes of symmetry collapse mechanisms lead to better upper bound solutions even though the boundary conditions have four planes of symmetry.

Upper bound calculations

For kinematically admissible mechanisms in associative soils, the rate of the internal plastic work $\dot{D}(\mathbf{v})$ is not less than the work rate of external forces

$$\int_{\Omega} \dot{D}(\mathbf{v}) d\Omega \geq \int_{\Gamma_p} \mathbf{p}^T \mathbf{v} d\Gamma_p + \int_{\Gamma_q} \mathbf{q}^T \mathbf{v} d\Gamma_q + \int_{\Omega} \boldsymbol{\gamma}^T \mathbf{v} d\Omega \tag{6}$$

where $\mathbf{v}$ is the kinematically admissible velocity vector, $\boldsymbol{\gamma}$ is unit weight vector, $\mathbf{p}$ is the limit load vector, $\mathbf{q}$ is the boundary stress (surcharge) vector, Ω is the volume of mechanism and

Γ is the surface that bounds the mechanism, the subscripts p and q refers to the respective boundaries for the limit load and boundary stress respectively.

If the surcharge and the distributed limit load are uniform and perpendicular to the boundaries and if the soil is uniform and subjected to gravitational acceleration then:

$$\int_{\Omega} \dot{D}(\mathbf{v}) d\Omega \geq -p \int_{\Gamma_p} \mathbf{n}_{\Gamma}^{T} \mathbf{v} d\Gamma_p - q \int_{\Gamma_q} \mathbf{n}_{\Gamma}^{T} \mathbf{v} d\Gamma_q + \gamma \int_{\Omega} \mathbf{n}_{\mathbf{g}}^{T} \mathbf{v} d\Omega \tag{7}$$

where $\mathbf{n}_{\Gamma}$ is outward unit vector normal to the boundary and $\mathbf{n}_{\mathbf{g}}$ is the acceleration direction vector.

In a cohesionless associative Mohr-Coulomb soil the rate of the internal plastic work $\dot{D}(\mathbf{v})$ vanishes. For $\gamma = 0$ and $c = 0$, the bearing capacity factor N_q' can then be evaluated from:

$$N_q' = \frac{\int_{\Gamma_q} \mathbf{n}_{\Gamma}^{T} \mathbf{v} d\Gamma_q}{-\int_{\Gamma_p} \mathbf{n}_{\Gamma}^{T} \mathbf{v} d\Gamma_p} \tag{8}$$

For $q = 0$ and $c = 0$, the bearing capacity factor N_γ' can be evaluated from:

$$N_\gamma' = \frac{-2\int_{\Omega} \mathbf{n}_{\mathbf{g}}^{T} \mathbf{v} d\Omega}{B\int_{\Gamma_p} \mathbf{n}_{\Gamma}^{T} \mathbf{v} d\Gamma_p} \tag{9}$$

It should be noted from figures 3 and 4 that the three-dimensional mechanism is assembled from regions of planar velocities and there are no out-of-plane velocities. Therefore, the out-of-plane plastic strain rate is zero (i.e. the intermediate principal strain rate is zero). Associative cohesive-frictional Mohr-Coulomb soil is assumed, and the boundary stress (the surcharge) is taken to be perpendicular to the boundary of the collapse mechanism. Michalowski [22] showed that under these conditions, equation 7 for a footing on a cohesive-frictional material could be rewritten as (see Appendix B):

$$\left(\int_{\Gamma_p} \mathbf{n}_{\Gamma}^{T} \mathbf{v} d\Gamma_p + \int_{\Gamma_q} \mathbf{n}_{\Gamma}^{T} \mathbf{v} d\Gamma_q \right) c \cot\phi \geq -p \int_{\Gamma_p} \mathbf{n}_{\Gamma}^{T} \mathbf{v} d\Gamma_p - q \int_{\Gamma_q} \mathbf{n}_{\Gamma}^{T} \mathbf{v} d\Gamma_q + \gamma \int_{\Omega} \mathbf{n}_{\mathbf{g}}^{T} \mathbf{v} d\Omega \qquad (10)$$

and the bearing capacity factor N_c' can be given by equation 5.

The least upper bound solution is obtained by optimisation the geometry of the collapse mechanism. It should be noted that the geometrical construction procedure implies that the inclinations of the cones (with the exception to the first cone) are not variable parameters in the optimisation of the mechanism. Thus, the projection of the mechanism in a vertical plane is quite different from the plane-strain mechanism. The variables in the optimisation procedures are the parameters ζ_1 and ζ_2, which determine the locations of the first cone apex, the independent angles α_1 and β_i (i=1, 2 …n-1) in each flank of the mechanism, where n is the number of rigid blocks in each flank. Because of the symmetry, only half of the mechanism was used in the upper bound calculations. Calculations were performed with 12 blocks in each of the three flanks of the half of the mechanism. Thus, the total number of unknown parameters for the optimisation process is 38. Increasing the number of blocks will not improve the solution significantly. For example, with 20 blocks per flank for L/B=1 and ϕ=30°-35°, the solution does not improve by more than 0.3%. The optimisation was carried out using the

MATLAB Optimization Toolbox. A geometrical constraint is imposed such that there are no common volumes between any two flanks of the mechanism. This is to ensure that the associative flow condition is satisfied everywhere within the proposed mechanism and the velocity field in each rigid block can be evaluated from the hodograph in Figure 4. In purely cohesive soils, Puzrin and Randolph [20] showed that using mechanisms with combined volumes could improve the upper bound solutions. However, this approach cannot be applied directly to frictional soils because of the restriction imposed by the normality rule. Figure 5 shows optimum mechanisms in cohesionless soil for L/B=2 at a relatively large angle of friction (ϕ=40°) and a smaller angle (ϕ=20°).

Results and discussion

Smooth footings on weightless cohesionless soils

Table 3 compares the least upper bound solution for N_q obtained from the 3D mechanism for L/B=25 with the plane-strain solution for a smooth strip footing of Reissner [12]. It should be noted that in both 2D and 3D analyses, N_q reaches 1.0 when the friction angle ϕ decreases to zero. In this table, the 3D mechanism gives consistent solutions with the 2D analysis, although it slightly overestimates the plane-strain analysis when ϕ >0. This discrepancy could be attributed to the kinematic constraint of the 3D mechanism, which has fewer independent parameters to optimise compared with the plane-strain mechanism. Table 4 lists the least upper bound for smooth rectangular footings expressed in term of the bearing capacity factor N_q' and the shape factor s_q. The results are presented for $10° \le \phi \le 40°$. N_q' is calculated using Equation 8. The shape factor s_q is calculated from Equation 2. For consistency, the results of the 3D mechanism for L/B=25 (the last Coulomb of Table 3) are taken to be equal to N_q in Equation 2. Figure 6 plots the shape factor s_q against the footing aspect ratio (L/B) for values of ϕ

between 10° and 40° in 5° intervals. Figure 6 shows that the shape factor s_q decreases with the increase of L/B and at large aspect ratio L/B the values of s_q converge towards 1.0.

Figures 7 compare the shape factor s_q estimated using the proposed 3D rigid-block mechanism with some of the previously published shape factors. The comparison was made for three values of angle ϕ: 15°, 25° and 35°. The literature on smooth rectangular footings is limited and scattered and comparison cannot be made directly with other published shape factors. The comparison was made with the rough footing solution of Michalowski [22], which is based on a rigid-block mechanism. The comparison was also made with the limit analysis finite element solution of [26] for rough footings in which a quadratic velocity field is used. The comparison was also made with the common empirical proposals for the shape factors of De Beer [10] (which is adopted in the specifications of the American Association of State Highway and Transportation Officials AASHTO [18]) and Meyerhof [3] and with the European design code EC7. It can be shown from these figures that the mechanism for smooth footings gives significantly lower values for the shape factor s_q compared with Michalowski's mechanism for rough footings. The current 3D analysis of smooth footings gives lower values for s_q values compared with the finite element limit analysis for rough footings except for square footings at high value of angle of frictions. Shape factors calculated using Meyerhof [3] and De Beer [10] methods fall close to one another, and they are consistently lower than those calculated from the upper bound mechanism for smooth footings.

Smooth footings on weightless cohesive-frictional soils

Table 5 the bearing capacity factor N_c' is calculated from N_q' using the linear transformation given by Equation 5. The upper bound solution for L/B=25 is used to obtain the shape factors

N_c using Equation 2. In the particular case of ϕ=0, the upper bound solutions obtained by the mechanism presented in this paper could be compared directly with the upper bound solution of Shield and Drucker [21] for smooth footings on cohesive soils as shown in Table 6. It should be noted that the linear transformation of Equation 5 cannot be used in soil without dilation. Thus, a nominal value of 10^{-5} degree is assigned to the angle of friction. Table 6 shows that the presented 3D mechanism gives solutions for N_c' which are in excellent agreement with Shield and Drucker [21]. This illustrates the usefulness of the linear transformation approach of [22] since the calculations of plastic work dissipation on every discontinuity surfaces in the mechanism is replaced by a much simpler surface integral. At L/B=25, the current 3D analysis gives N_c'=5.174 which is only about 0.1% higher than that predicted by Shield and Drucker [21] and only about 0.6% higher than the exact value of 2+π for plane-strain footings. The exact values of N_c' for a strip footing at different angles of friction are shown in Table 7. These values were calculated using the ABC software of Martin [8]. Table 7 demonstrates that the 3D upper bound mechanism gives consistent results compared to the exact 2D solutions. These results could justify the use of values at L/B=25 in the 3D analysis as references in the calculations of the shape factors.

Comparison is also made with the lower bound finite element limit analysis of Yang et al. [27] and Lyamin and Sloan [28] for smooth rectangular footings. It should be noted that the Drucker-Prager model was adopted in Yang et al. [27] and the collapse loads were calculated for three different yield conditions (as shown in Figure 8): (i) DP I where Drucker-Prager yield condition is an inscribed circle located inside the hexagon of Mohr-Coulomb yield condition in the π-plane, (ii) DP II where the Drucker-Prager yield condition is a circle that has the same closed area as the hexagon of Mohr-Coulomb yield condition in the π-plane, and (iii) DP III where the Drucker-Prager yield condition is a circumcircle of the hexagon of Mohr-Coulomb

yield condition in the π-plane. Comparison with lower bound solutions is given in Table 8 for footings on purely cohesive soils and in Table 9 for footings on cohesive-frictional soils. All 3D upper bound solutions are higher than the corresponding lower bound results given by Lyamin and Sloan [28]. The 3D upper solutions and the lower bound solutions of Lyamin and Sloan [28] are obtained using Mohr-Coulomb yield criterion and therefore, the true solution should be between the upper and lower bound theoretically. It can be seen from Tables 8 and 9 that the lower bound solutions, in which Mohr-Coulomb yield condition is adopted, fall between DP I and DP II lower bound solutions when L/B equal to 1 and 2 in purely cohesive soils and when L/B equal to 1 in the case of cohesive-frictional soils. Mohr-Coulomb upper bound solutions are higher than the corresponding DP I and DP II Drucker-Prager lower bound results. The lower bound formulation with DP III yield condition can give unreliable estimates for the collapse loads of smooth rectangular footings. In purely cohesive soils, DP III gives higher N_c' compared to Mohr-Coulomb upper bound solution for all values of L/B with the exception of footings with L/B=10 (Table 8).

Figure 9 shows that the shape factor s_c increases with the decrease in L/B and at large L/B s_c converge towards 1.0. Comparison was made with the rough footing solutions and with empirical proposals, as shown in Figure 10. The UB solution obtained using the collapse mechanism for smooth footing is compared with the upper bound solution of Michalowski [22] for rough footings and the finite element analysis of Michalowski and Dawson [23]. It should be noted that conventional finite element method offers an approximate solution which is not necessarily to be strict upper or lower bound to collapse loads. Figure 10 shows that shape factors s_c calculated from the smooth footing mechanism are significantly lower than the upper bound mechanism for rough footings. The smooth footing mechanism gives factors lower than the finite element analysis of Michalowski and Dawson [23] except for square footings

(L/B=1). Shape factors calculated using Meyerhof [3] and De Beer [10] methods fall very close to one another, and they are lower than those calculated from the upper bound mechanism for smooth footing. EC7 ignores the influence of the friction angle ϕ on s_c and significantly underestimates the shape factor compared with other empirical and analytical methods for both rough and smooth footing.

Smooth footings on cohesionless soils with self-weight

The limit analysis of soil with self-weight is complicated by the fact that the shear strength increases with depth from a value of zero at the ground surface [5]. This implies that any velocity discontinuity should be curved which straight velocity discontinuities could be assumed in the analysis of weightless soil. This means that any collapse mechanism with straight velocity discontinuities, such as Prandtl and Hill type mechanisms and the rigid-block mechanisms of Michalowski [7][22] and Soubra [15], are not capable of yielding exact solutions. They can only give upper bound to the correct collapse loads. Similar conclusions could be drawn regarding the mechanism for smooth rectangular footings presented in this paper.

Figure 11 compares the least upper bound solution for N_γ obtained from the 3D mechanism for L/B=25 with analytical and empirical solutions for a strip footing. The comparison is made with the best-known rigid-block upper bound plane-strain solution of Michalowski [7] for smooth strip footing and with made with the 'exact' the method of characteristics analysis of Martin [8]. Comparison is also made with two common proposals for N_γ: Meyerhof [3], Vesic [4], which is adopted in AASHTO design code [18] and with EC7 [17]. This figure shows that the 3D mechanism gives consistent solutions with the plane-strain upper bound analysis of Michalowski [7] although it slightly overestimates the plane-strain analysis. It also

overestimates the exact method of characteristics solution of Martin [8]. On the contrary, the 3D mechanism for smooth footings gives lower values for N_γ compared with values suggested by Meyerhof [3], Vesic [4] (and AASHTO), and EC7. It is interesting to note that the EC7 recommendation for N_γ is about 250% higher than the value predicted by the method of characteristics of Martin [8].

Table 10 lists the least upper bound for smooth rectangular footings expressed in term of the bearing capacity factor N'_γ and the shape factor s_γ. The calculations were carried out with c=0 and q=0. The results are presented for $10° \le \phi \le 40°$. N'_γ is calculated using Equation 8. The shape factor s_γ is calculated from Equation 2 with the results of the 3D mechanism at L/B=25, c=0 and q=0 are taken to be equal to N_γ. Figure 12 plots the shape factor s_γ against the normalised footing dimension. Figure 12 shows that at large aspect ratio L/B the values of s_γ converge towards 1.0. The values of s_γ decrease with the decrease of L/B at small angles of friction ($\phi \le 20°$) and becomes less than 1.0 at small aspect ratios while increases with L/B at bigger angles of friction ($\phi > 20°$).

Figures 13 compare the shape factors s_γ estimated using the proposed 3D rigid-block mechanism the 3D rough footing solution of Michalowski [22], the advanced finite element solution of [26] Meyerhof [3], Brinch Hansen [11] and with the design code EC7. It can be shown from the figure that the mechanism for smooth footings gives significantly lower values for s_γ with Michalowski's mechanism for rough footings. However, the limit analysis finite element analysis of [26] for rough footings gives slightly lower s_γ. Meyerhof [3] gives an inconsistent solution for s_γ. At small angles of friction, it implies that the shape factor increases with the decrease of L/B, which contradicts the results of the smooth mechanism and the other

published solutions. The upper bound solutions for smooth soil-footing interface suggest that s_γ is influenced by ϕ which is consistent with the limit analysis solutions of rough footings of Michalowski [22] and Antão et al. [26] but disagrees with EC7 and Brinch Hansen, which suggests that s_γ is a function of L/B only.

Conclusions

Rigorous upper bound solutions for smooth rectangular footings on frictional materials are presented. These solutions were derived using a three-dimensional collapse mechanism composes of rigid-block truncated by conical surfaces. The three-dimensional mechanism is assembled from regions of planar velocities with no out-of-plane velocities. The velocity field is kinematically admissible. The soil is taken to yield according to associative Mohr-Coulomb failure criterion, and the velocity vectors are inclined at an angle ϕ to the discontinuity surfaces separating the mechanism from the soil at rest and therefore, satisfy the normality requirement.

The numerical results of the shape factors are presented in the form of design charts for practical use in geotechnical engineering. The results suggest that the shape factors depend on the roughness of the footing-soil interface. This needs to be considered in designing shallow foundations. The bearing capacities of smooth-based footings are lower than those of perfectly rough footings.

The upper bound approach with rigid-block collapse mechanisms is a useful tool to obtain rigorous solutions for collapse loads in footings and to visualise the deformation mechanisms associated with these loads. The kinematical admissibility imposes constraints on the geometry of the presented collapse mechanism. Thus, it might be possible to obtain improved upper bound solutions for smooth rectangular footings on frictional materials using numerical

techniques such as the limit analysis finite element method [34] and the discontinuity layout optimisation (DLO) algorithm [35]. Nevertheless, the presented rigid-block mechanism could provide benchmarks to valid such solutions.

Acknowledgements

The author would like to acknowledge the financial support of the UK Engineering and Physical Sciences Research Council (Grant EP/P029434/1).

Appendix A

For the projection of a flank of the mechanism on the vertical x-z plane shown in Fig. 4, if Cartesian coordinates system is used with the origin taken at the apex of the first cone, then for any point on the shown ellipse at the discontinuity face its coordinates (x_i, y_i, z_i) satisfies the following equations:

$$\frac{x_V - x_i}{x_V - \zeta_1 B} = \frac{z_V - z_i}{z_V} \tag{11}$$

$$y_i = \pm\sqrt{\left(n_x\left(x_i - x_o\right) + n_z\left(z_i - z_o\right)\right)^2 \sec^2\phi - \left(x_i - x_o\right)^2 - \left(z_i - z_o\right)^2} \tag{12}$$

where $(x_O, 0, z_O)$ are the coordinates of the apex of the cone (point A_i), $(x_V, 0, z_V)$ is the coordinates of point V and $\{n_x \quad 0 \quad n_z\}^T$ is a unit vector giving the direction of the axis of the cone.

The area of the ellipsoidal cross section (the area shaded with grey colour) is given by:

$$\Gamma_E = \frac{ab}{2}\left(-\left(1-\frac{d}{a}\right)\sqrt{2\frac{d}{a}-\frac{d^2}{a^2}} + cos^{-1}\left(1-\frac{d}{a}\right)\right) \tag{13}$$

The volume of truncated cone *i* is then given by:

$$\Omega_i = \frac{1}{3}\Gamma_E h - \Omega_{i-1} \tag{14}$$

where the dimensions *a* and *b* are the ellipse major and minor axis, respectively, *d* is the height of the elliptical segment and *h* is the height of the cone as shown in Figure 4.

Appendix B

Michalowski [22] has shown the calculations of work dissipation rate on the velocity discontinuity surfaces and within the deformation regions of the soil can be replaced by a much simpler surface integral if the following three conditions are satisfied: (i) the soil plasticity obeys associative cohesive-frictional Mohr-Coulomb yield criterion (ii) the boundary stress is taken to be perpendicular to the boundary of the collapse mechanism and (iii) the intermediate principal plastic strain rate is zero ($\dot{\varepsilon}_2 = 0$). A summary of the mathematical derivation is given in this appendix, for detailed discussion, the reader should refer to [22].

The rate of the internal plastic work per unit volume $\dot{D}(\mathbf{v})$ in an associative Mohr-Coulomb material is given by:

$$\dot{D}(\mathbf{v}) = \left(\dot{\varepsilon}_1 - \dot{\varepsilon}_3\right) c \cos\phi \tag{15}$$

where $\dot{\varepsilon}_1$ and $\dot{\varepsilon}_3$ are the major and the minor principal plastic strain rate, respectively.

The associative flow rule implies that:

$$\frac{\dot{\varepsilon}_1 + \dot{\varepsilon}_3}{\dot{\varepsilon}_1 - \dot{\varepsilon}_3} = -\sin\phi \tag{16}$$

In the case of $\dot{\varepsilon}_2 = 0$, substituting equation 16 into 15 gives:

$$\dot{D}(\mathbf{v}) = -\dot{\varepsilon}_v c\cot\phi = \mathrm{div}(\mathbf{v})c\cot\phi \tag{17}$$

where $\dot{\varepsilon}_v$ is the volumetric plastic strain rate and $\mathrm{div}(\mathbf{v})$ is the divergence of the velocity vector.

The integral of the plastic volumetric strain rate in the entire volume Ω of the mechanism can be transformed to a surface integral over the boundary Γ of the mechanism using the divergence theorem:

$$\int_{\Omega} \dot{\varepsilon}_v d\Omega = -\int_{\Omega} \mathrm{div}(\mathbf{v}) d\Omega = -\int_{\Gamma} \mathbf{n}_{\Gamma}^{T}\mathbf{v} d\Gamma \tag{18}$$

Surface Γ bounding the mechanism can be divided into part Γ_q where the stress condition is known and part Γ_p where the velocity boundary condition is known. Therefore, the integral of the internal plastic work in the entire mechanism can be given by:

$$\int_{\Omega} \dot{D}(\mathbf{v}) d\Omega = -\int_{\Omega} \dot{\varepsilon}_v c\cot\phi d\Omega = \left(\int_{\Gamma_p} \mathbf{n}_{\Gamma}^{T}\mathbf{v} d\Gamma_p + \int_{\Gamma_q} \mathbf{n}_{\Gamma}^{T}\mathbf{v} d\Gamma_q \right) c\cot\phi \tag{19}$$

References

[1] Terzaghi K. Theoretical soil mechanics. John Wiley and Sons Inc; 1943.

[2] Caquot, A., and Kerisel, J. Sur le terme de surface dans le calcul des fondations en milieu pulverulent. Proc., 3rd Int. Conf. Soil Mechanics Found. Eng., Vol. 1, Zürich, Switzerland, 336–337. 1953.

[3] Meyerhof GG. Some recent research on bearing capacity of foundations. Can Geotech J 1963; 1(1):16–26.

[4] Vesic AS. Analysis of ultimate loads of shallow foundations. ASCE J Soil MechFound Div 1973; 99(1):45–73.

[5] Chen, W. F. Limit analysis and soil plasticity. Elsevier Scientific Publishing Company, London; 1975.

[6] Bolton, M. D., and Lau, C. K. Vertical bearing capacity factors for circular and strip footings on Mohr-Coulomb soil." Can. Geotech. J. 1993;30: 1024–1033.

[7] Michalowski RL. An estimate of the influence of soil weight on bearing capacity using limit analysis. Soils Found 1997;37 (4):57–64.

[8] Martin CM. Exact bearing capacity calculations using the method of characteristics. In: Proc. 11th int. conf. IACMAG, vol. 4, Turin; 2005. p. 441-450.

[9] Salgado R. The engineering of foundations. McGraw-Hill; 2008.

[10] De Beer EE. Experimental determination of the shape factors and the bearing capacity factors of sand. Géotechnique 1970; 20:387–411.

[11] Brinch Hansen J. A revised and extended formula for bearing capacity. Bull Danish Geotech Inst 1970; 28:5–11.

[12] Reissner, H. Zum Erddruckproblem." Proc., 1st Int. Congress for Applied Mechanics, C. B. Biezeno and J. M. Burgers, eds., Delft,The Netherlands, 1924; 295–311.

[13] Caquot, A. I. Équilibre des massifs á frottement interne, Stabilité des terres pulvérulentes et cohérentes, Gauthier-Villars, Paris; 1934.

[14] Smith, C. C. Complete limiting stress solutions for the bearing capacity of strip footings on a Mohr–Coulomb soil. . Géotechnique 2005; 55(8): 607–612.

[15] Soubra A-H. Upper-bound solutions for bearing capacity of foundations. J. Geotechn. Geoenviron. Engng. ASCE 1998 125 (1): 59–68.

[16] Hjiaj M. Lyamin A V, Sloan SW. Numerical limit analysis solutions for the bearing capacity factor N_γ. Int. J. Solid. Struct. 2005;42:1681–1704.

[17] Eurocode 7. Geotechnical design, part 1: general rules. CEN, European Committee for Standardization, Brussels; 2004.

[18] AASHTO. AASHTO LRFD Bridge Design Specifications, 8th Edition. American Association of State Highway and Transportation Officials , Washington DC. , 2017, www.transportation.org.

[19] Michalowski, R. L. Rule of equivalent states in limit state analysis of soils. J. Geotech. Geoenviron. Eng. 2001; 127(1): 76–83.

[20] Puzrin A. M.and Randolph M F. On the superposition of plastically dissipated work in upper bound limit analysis. Proc. R. Soc. Lond. A (2001) 457, 567–586

[21] Shield, R. T., and Drucker, D. C. The application of limit analysis to punch indentation problems. J. Appl. Mech. 1953; (20): 453–460.

[22] Michalowski RL. Upper-bound load estimates on square and rectangular footings. Géotechnique 2001; 51(9):787–98.

[23] Michalowski, R.L. and Dawson, E.M. Three-dimensional analysis of limit loads on Mohr-Coulomb soil. Foundations of Civil and Environmental Engineering 2002; (1):1, 137-147.

[24] Zhu M, Michalowski RL. Shape factors for limit loads on square and rectangular footings. ASCE J Geotech Geoenviron Eng 2005;131(2):223–31.

[25] Lyamin, A. V. Salgado R, Sloan S W and Prezzi M. Two- and three-dimensional bearing capacity of footings in sand. Géotechnique 2007;57(8): 647–662.

[26] Antão A.N. Vicente da Silva M., Guerra N. and Delgado R.An upper bound-based solution for the shape factors of bearing capacity of footings under drained conditions using a parallelized mixed f.e. formulation with quadratic velocity fields Comput. Geotech. 2012; 41:23–35.

[27] Yang H, Shen Z and Wang J. 3D lower bound bearing capacity of smooth rectangular surface footings. Mech. Res. Commun. 2003; (30): 481–492.

[28] Lyamin AV & Sloan SW. (2000). Rigorous lower bound solutions for the Bearing capacity of rectangular foundations. ISRM Int. Symp. 19-24 November, Melbourne, Australia. ISRM-IS-2000-200

[29] Gourvenec S Randolph MF & Kingsnorth O. Undrained Bearing Capacity of Square and Rectangular Footings. Int. J. Geomech. 2006;6 (3):147-157.

[30] Hill R. The Mathematical Theory of Plasticity. Oxford University Press 1950.

[31] Prandtl, L. Eindringungsfestigkeit und festigkeit von schneiden. Angew. Math. U. Mech 1921, 1:15–20.

[32] Leca, E., and Dormieux, L. Upper and lower bound solutions for the face stability of shallow circular tunnels in frictional material. Géotechnique 1990; 40 (4):581–606.

[33] Soubra A-H & Regenass P. Three-dimensional passive earth pressures by kinematical approach. J. Geotechn. Geoenviron. Engng. ASCE 2000; 126 (11):969-978.

[34] Sloan S W. Geotechnical Stability Analysis. Géotechnique; 63(7):531–571.

[35] Smith C, Gilbert M. Application of discontinuity layout optimization to plane plasticity problems. Proc. Royal Soc. Lond. A.: mathematical, physical and engineering sciences2007; 463(2086): 2461–84.

Table1: Common proposals for the bearing capacity factor N_γ

Proposal	N_γ
Caquot and Kerisel [2] and Vesic [4]	$N_\gamma = 2\left(N_q + 1\right)\tan\phi$

Meyerhof [3]	$N_\gamma = \left(N_q - 1\right)\tan\left(1.4\phi\right)$
Brinch Hansen [11]	$N_\gamma = 1.5\left(N_q - 1\right)\tan\phi$
Chen [5]	$N_\gamma = 2\left(N_q + 1\right)\tan\phi\tan\left(\frac{\pi}{4} + \frac{\phi}{5}\right)$
Salgado [9]*	$N_\gamma = \left(N_q - 1\right)\tan\left(1.32\phi\right)$
EC7 [17]	$N_\gamma = 2\left(N_q - 1\right)\tan\phi$

*For rough footing only

Table2: Common proposals for the shape factors

Proposal	s_q	s_γ	s_c
Meyerhof [3]	$s_q = 1 + 0.1K_p\frac{B}{L}$	$s_\gamma = 1 + 0.1K_p\frac{B}{L}$	$s_c = 1 + 0.2K_p\frac{B}{L}$

Vesic [4] and De Beer [10]	$s_q = 1 + \frac{B}{L}\tan\phi$	$s_\gamma = 1 - 0.4\frac{B}{L}$	$s_c = 1 + \frac{N_q}{N_c}\frac{B}{L}$
Brinch Hansen [11]	$s_q = 1 + \frac{B}{L}\sin\phi$	$s_\gamma = 1 - 0.4\frac{B}{L}$	$s_c = 1 + 0.2\frac{B}{L}$
EC7 [17]	$s_q = 1 + \frac{B}{L}\sin\phi$	$s_\gamma = 1 - 0.3\frac{B}{L}$	$s_c = 1 + 0.2\frac{B}{L}$

Note: $K_p = \frac{1+\sin\phi}{1-\sin\phi}$

Table3: Baring capacity factor N_q for strip footings: comparison between plane-strain and 3D analyses

Angle of friction ϕ: degrees	Plane-strain analysis Reissner [12]	3D analysis L/B=25

0	1.000	1.000
5	1.568	1.573
10	2.471	2.491
15	3.941	3.999
20	6.399	6.552
25	10.662	11.052
30	18.401	19.391
35	33.296	35.949
40	64.195	73.988

Table 4: Baring capacity of rectangular footings (c=0 and γ=0)

ϕ (°)	L/B=1		L/B=2		L/B=3		L/B=5		L/B=10	
	N'_q	s_q	N'_q	s_q	N'_q	s_q	N'_q	s_q	N'_q	s_q

10	2.841	1.140	2.673	1.073	2.610	1.048	2.558	1.027	2.516	1.010
15	5.043	1.261	4.539	1.135	4.353	1.089	4.196	1.049	4.074	1.019
20	9.403	1.435	8.009	1.222	7.506	1.146	7.084	1.081	6.756	1.031
25	18.552	1.679	14.829	1.342	13.515	1.223	12.425	1.124	11.577	1.048
30	38.902	2.006	29.080	1.500	25.685	1.325	22.891	1.180	20.728	1.069
35	90.761	2.525	62.811	1.747	53.268	1.482	45.501	1.266	39.579	1.101
40	316.740	4.281	196.960	2.662	151.500	2.048	119.250	1.612	89.346	1.208

Table 5: Baring capacity of rectangular footings (q=0 and γ=0)

ϕ (°)	L/B=1	L/B=2	L/B=3	L/B=5	L/B=10

	N_c'	s_c	N_c'	s_c	N_c'	s_c	N_c'	s_c	N_c'	s_c
10^{-5}	5.711	1.104	5.450	1.053	5.360	1.036	5.281	1.021	5.214	1.008
5	7.5764	1.157	7.083	1.082	6.898	1.054	6.742	1.030	6.621	1.011
10	10.441	1.235	9.488	1.122	9.131	1.080	8.836	1.045	8.598	1.017
15	15.089	1.348	13.208	1.180	12.514	1.118	11.928	1.066	11.472	1.025
20	23.087	1.513	19.257	1.262	17.875	1.172	16.716	1.096	15.814	1.037
25	37.640	1.746	29.656	1.376	26.839	1.245	24.501	1.137	22.682	1.052
30	65.648	2.061	48.636	1.527	42.756	1.342	37.916	1.190	34.170	1.073
35	128.192	2.568	88.275	1.769	74.646	1.496	63.554	1.273	55.097	1.104
40	376.284	4.326	233.536	2.685	179.359	2.062	140.925	1.620	105.287	1.210

Table 6: Comparison with the Upper Bound solution of Drucker and Shield for smooth footings on purely cohesive soil

	L/B=1	L/B=2	L/B=3	L/B=5	L/B=10	L/B=25
Current analysis	5.711	5.450	5.360	5.281	5.214	5.174
Shield and Drucker [21]	5.711	5.469	5.360	5.273	5.207	5.168

Table 7: Baring capacity factor N_c for strip footings: comparison between plane-strain and 3D analyses

Angle of friction ϕ: degrees	Plane-strain analysis Martin [8]	3D analysis L/B=25
10^{-5}	5.142	5.174
5	6.489	6.5474
10	8.345	8.456
15	10.977	11.191
20	14.837	15.254
25	20.721	21.557
30	30.140	31.854
35	46.124	49.912
40	75.313	86.984

Table 8: Comparison with lower-bound solutions for smooth footings on purely cohesive soil

	Yang et al. [27] (Lower Bound)			Lyamin and Scott [28] (Lower Bound) MC	Current analysis (Upper Bound) MC
	DP I	DP II	DP III		
L/B=1	5.256	5.567	6.174	5.31	5.711
L/B=2	5.014	5.306	5.856	5.20	5.450
L/B=5	4.782	4.952	5.354	5.12	5.281
L/B=10	4.458	4.831	5.166	-	5.214

Table 9: Comparison with lower-bound solutions for smooth footings on weightless cohesive-frictional soil (q=0 and γ=0)

ϕ (°)		Lower Bound solution Yang et al. [27]			Lyamin and Scott [28] (Lower Bound) MC	Current analysis (Upper Bound) MC
		DP I	DP II	DP III		
10	L/B=1	8.962	9.774	12.088	9.02	10.441
	L/B=2	6.193	6.899	8.719	8.64	9.488
	L/B=5	-	-	-	8.34	8.836
15	L/B=1	10.972	12.088	17.129	-	15.089
	L/B=2	8.519	9.587	13.771	-	13.208
20	L/B=1	16.385	19.465	31.460	17.47	23.087
	L/B=2	10.668	12.717	21.115	16.10	19.257
	L/B=5	-	-	-	14.99	16.716
25	L/B=1	20.976	26.994	52.712	-	37.640
	L/B=2	12.200	14.992	31.179	-	29.656
30	L/B=1	31.117	42.065	116.327	-	65.648
	L/B=2	15.246	22.719	64.386	-	48.636

Table 10: Baring capacity of rectangular footings (c=0 and q=0)

ϕ (°)	L/B=1		L/B=2		L/B=3		L/B=5		L/B=10	
	N'_γ	s_γ	N'_γ	s_γ	N'_γ	s_γ	N'_γ	s_γ	N'_γ	s_γ
10	0.344	0.753	0.403	0.882	0.422	0.925	0.438	0.959	0.450	0.985
15	0.962	0.832	1.066	0.922	1.099	0.951	1.126	0.973	1.145	0.990
20	2.495	0.952	2.571	0.981	2.591	0.989	2.606	0.994	2.615	0.998
25	6.465	1.124	6.129	1.066	5.998	1.043	5.889	1.024	5.804	1.009
30	17.396	1.363	15.068	1.181	14.259	1.117	13.589	1.065	13.075	1.025
35	50.157	1.692	39.698	1.339	36.117	1.218	33.211	1.120	30.997	1.045
40	189.240	2.481	131.400	1.723	111.400	1.461	95.525	1.253	83.420	1.094

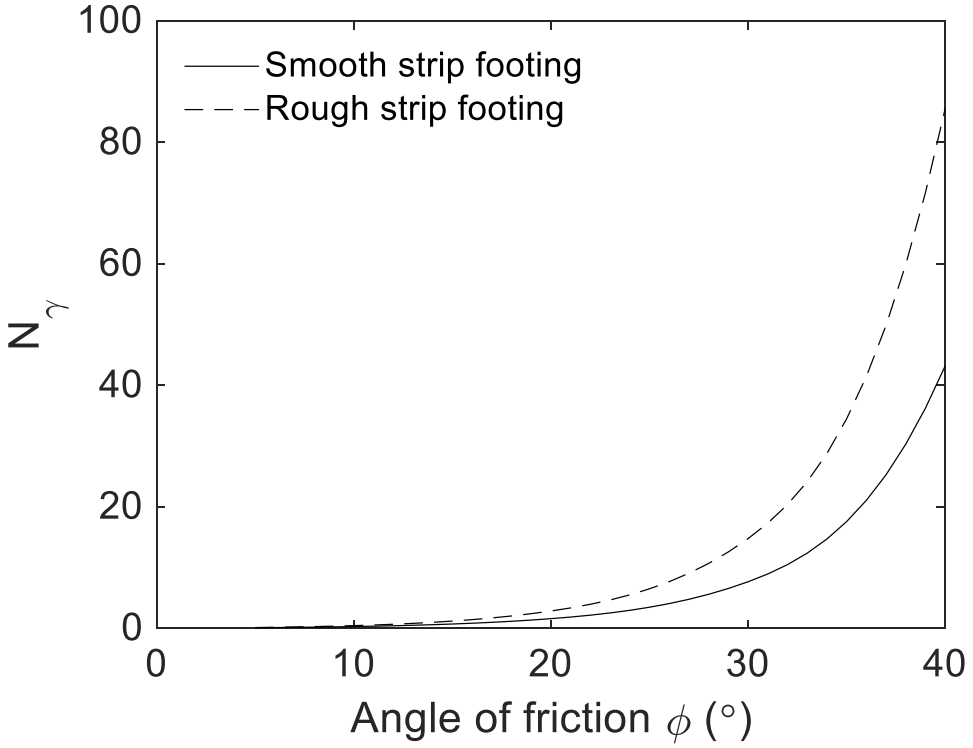

(a)

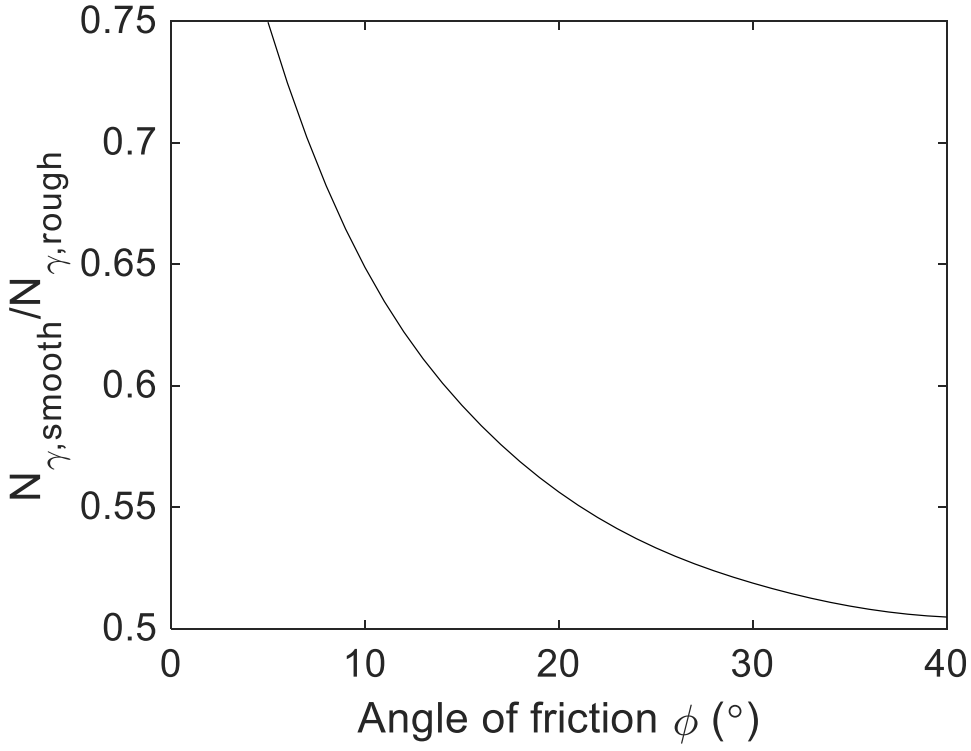

(b)

Figure 1: Effect of the footing roughness on the bearing capacity of a strip footing (values of N_γ are by calculated using the ABC software [8])

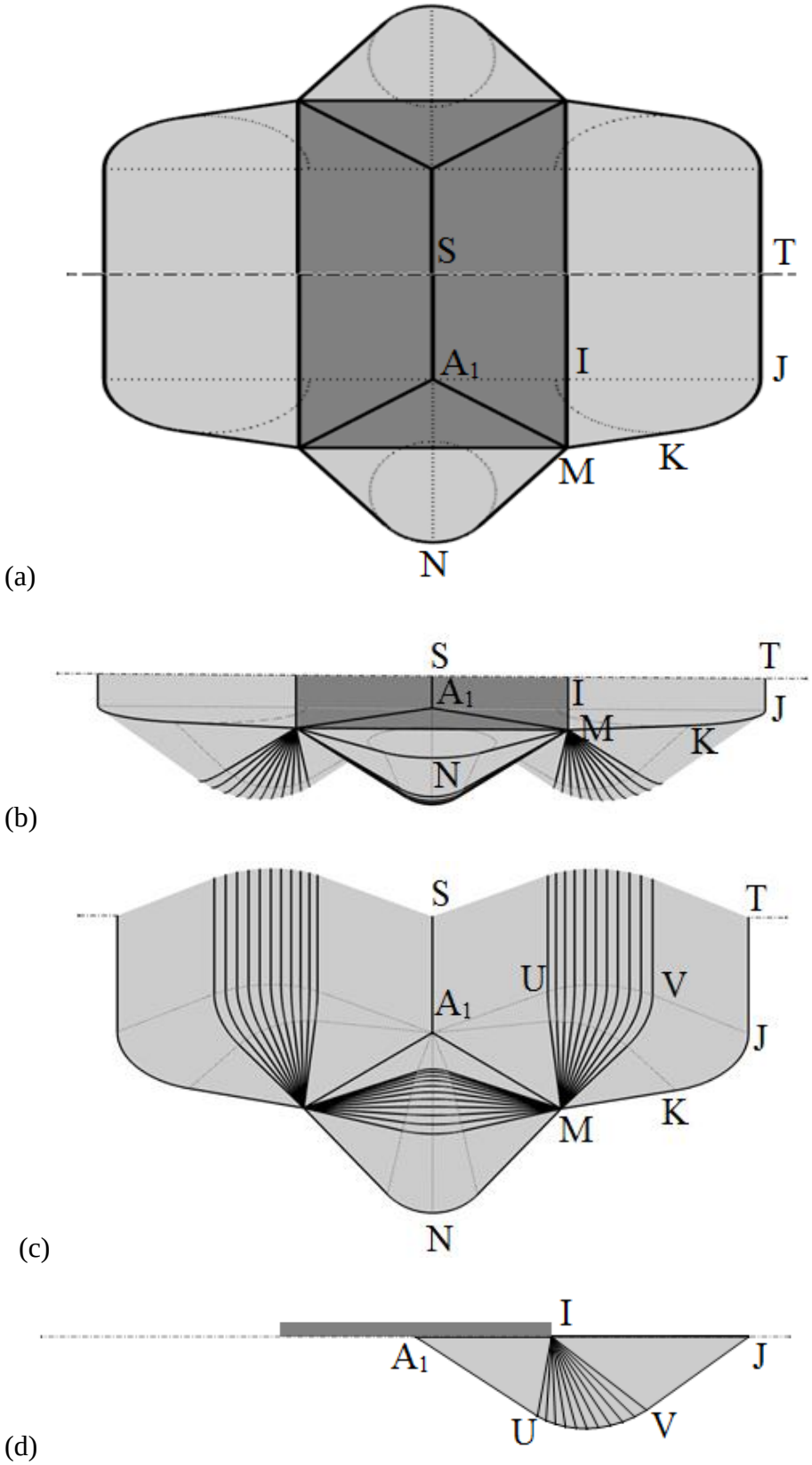

Figure 2: 3D collapse mechanism for a smooth rectangular footing on frictional material. (a) top view (b) front view (c) view from the bottom (d) a projection of the mechanism on a vertical plane.

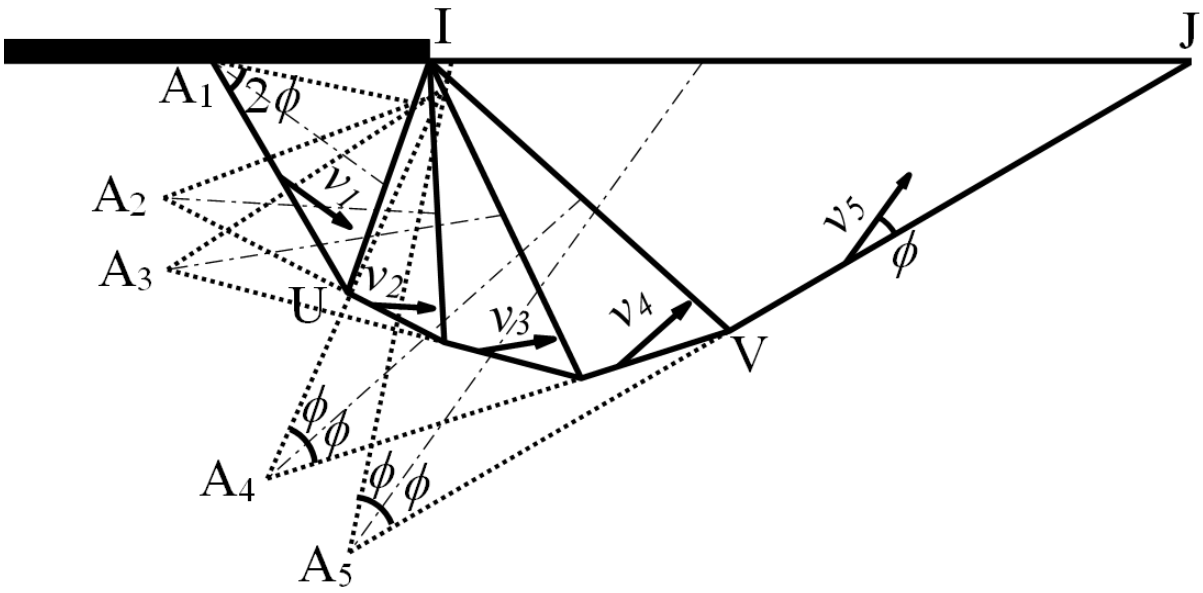

(a)

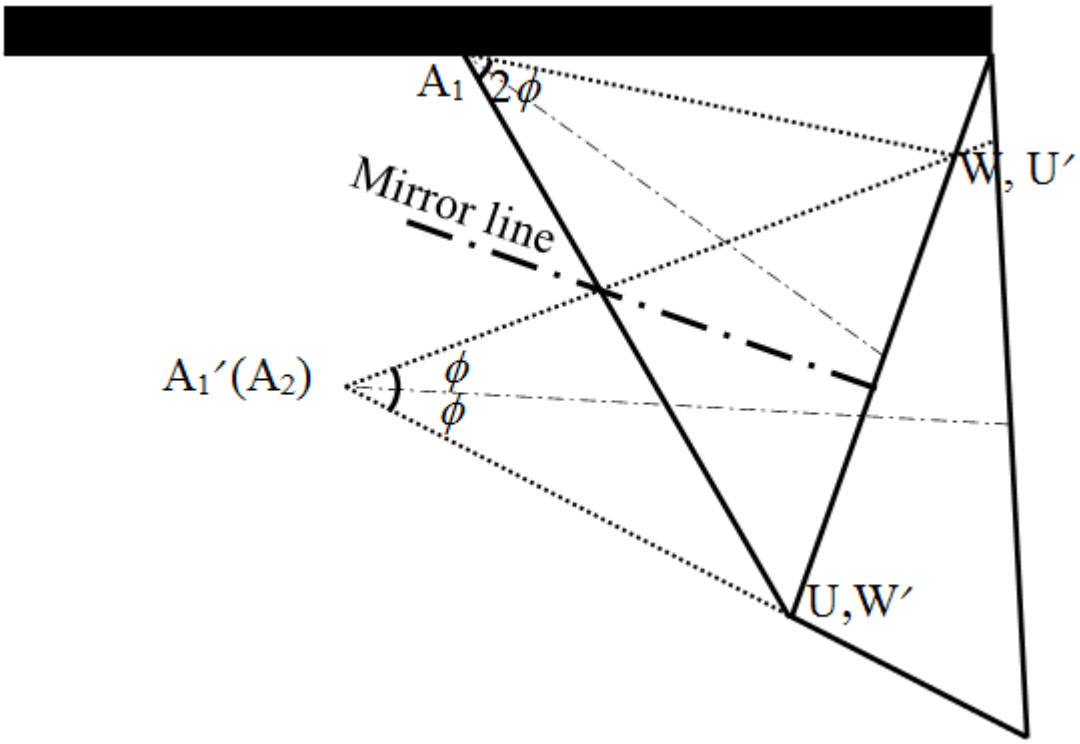

(b)

Figure 3: Multi-block mechanism (a) kinematic admissibility of the mechanism (b) construction of the first two rigid blocks

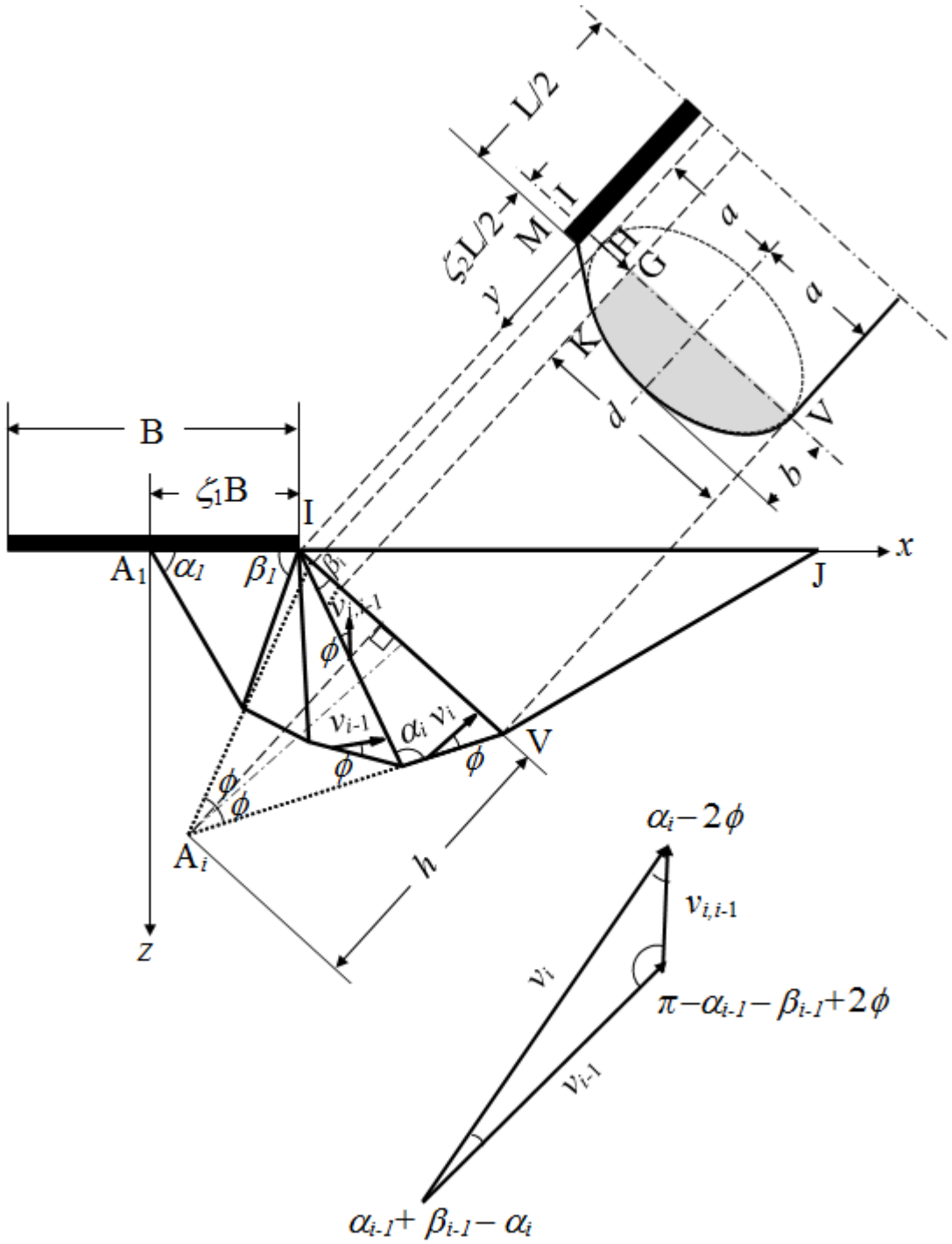

Figure 4: Variable parameters for the multi-block mechanism

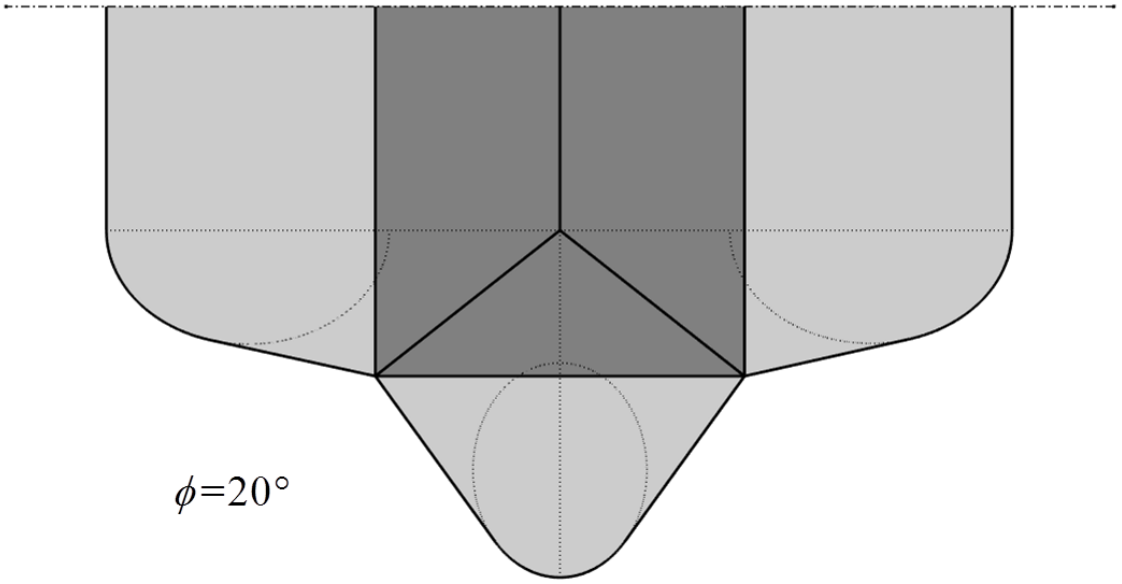

(a)

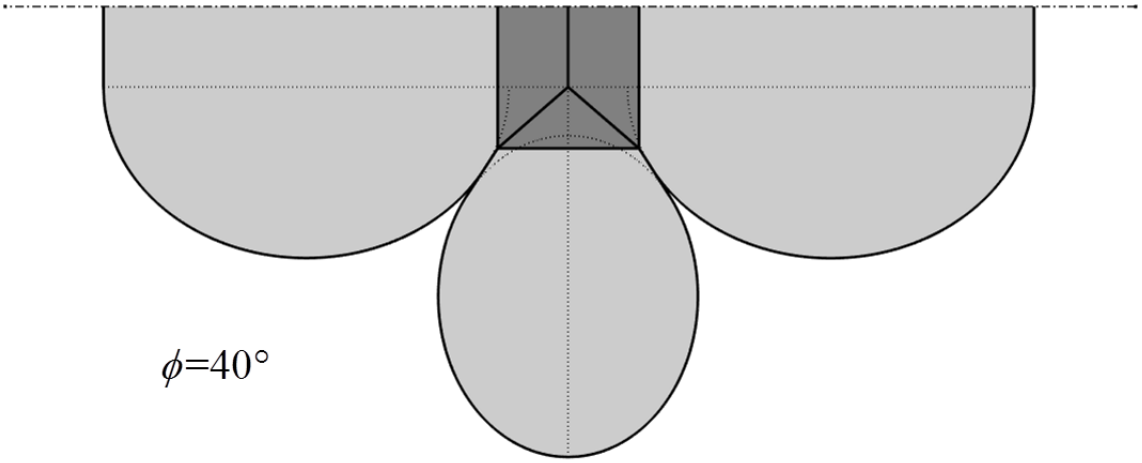

(b)

Figure 5: Patterns of the multi-block mechanism, L/B=2, q=0 and c=0: (a) ϕ =20° (b) ϕ =40°

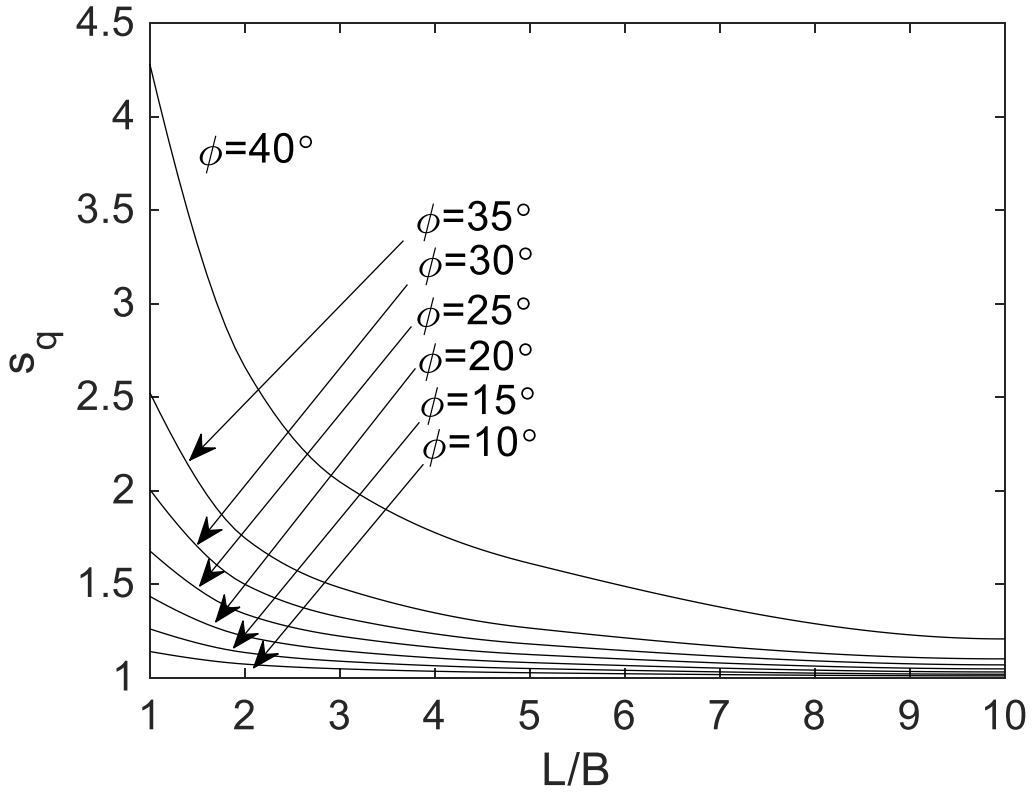

Figure 6: Values of shape factor s_q in smooth rectangular footings

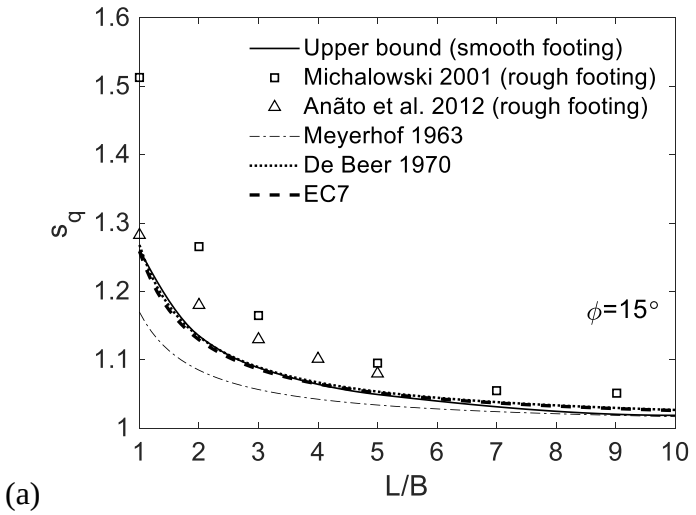

(a)

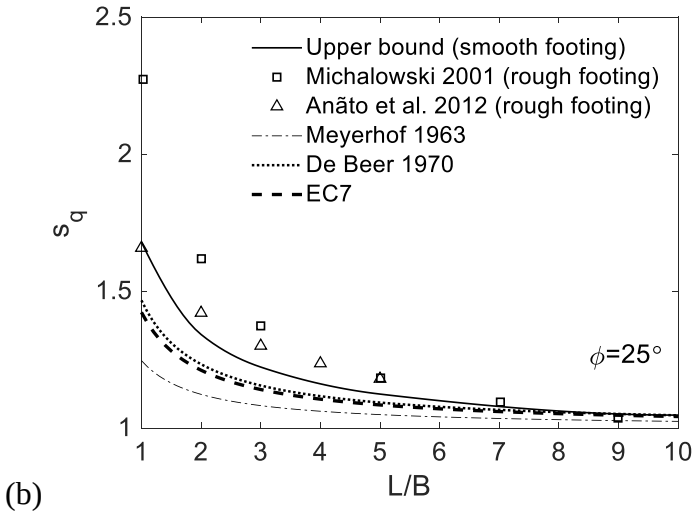

(b)

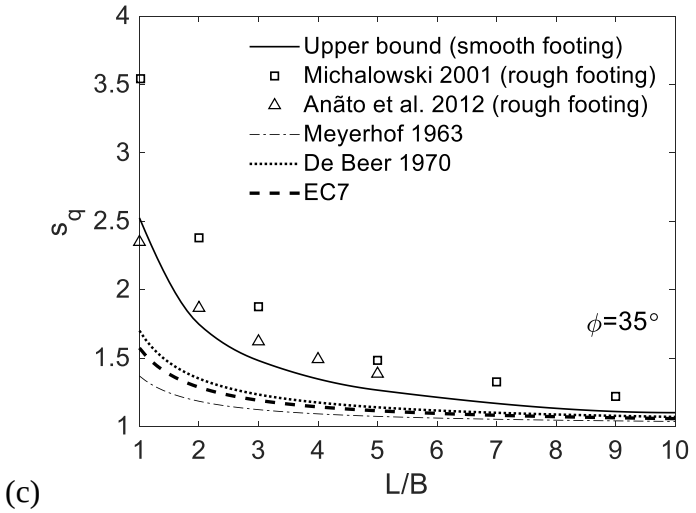

(c)

Figure 7: Values of shape factor s_q : comparison with previously published results (a) ϕ =15° (b) ϕ =25° (c) ϕ =35°

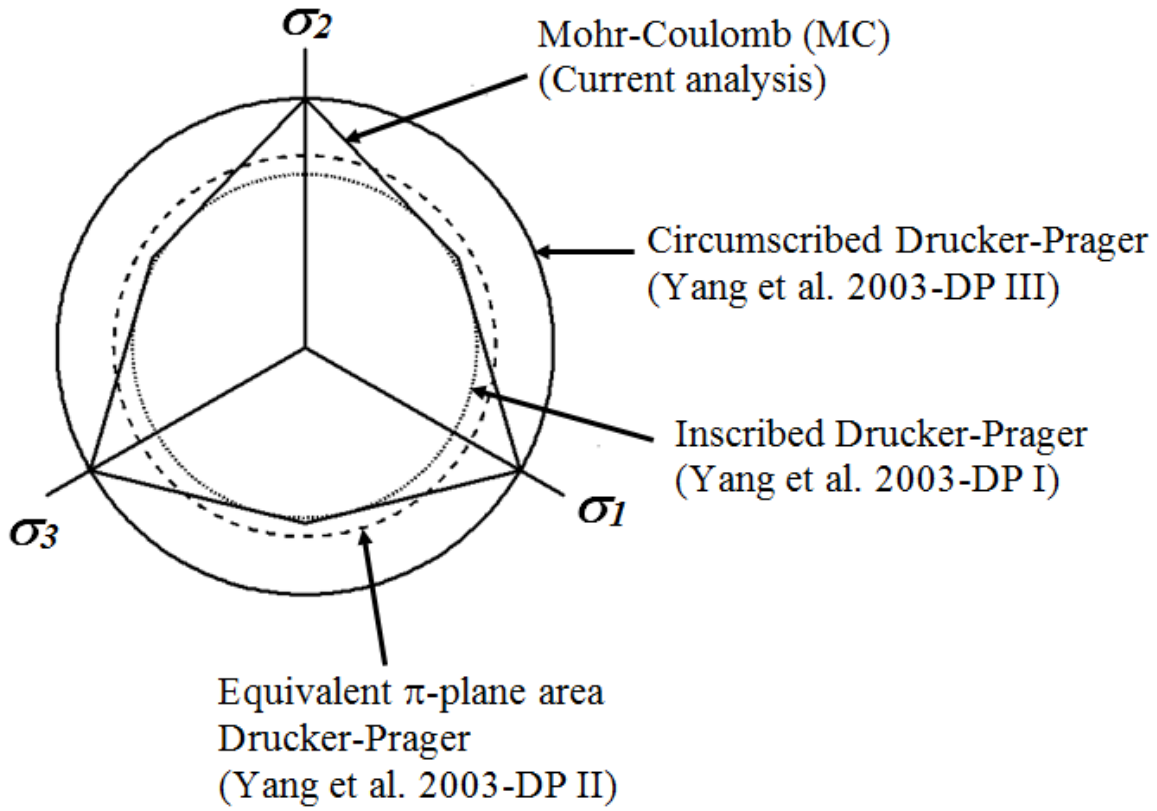

Figure 8: Comparison of limit analysis yield criteria.

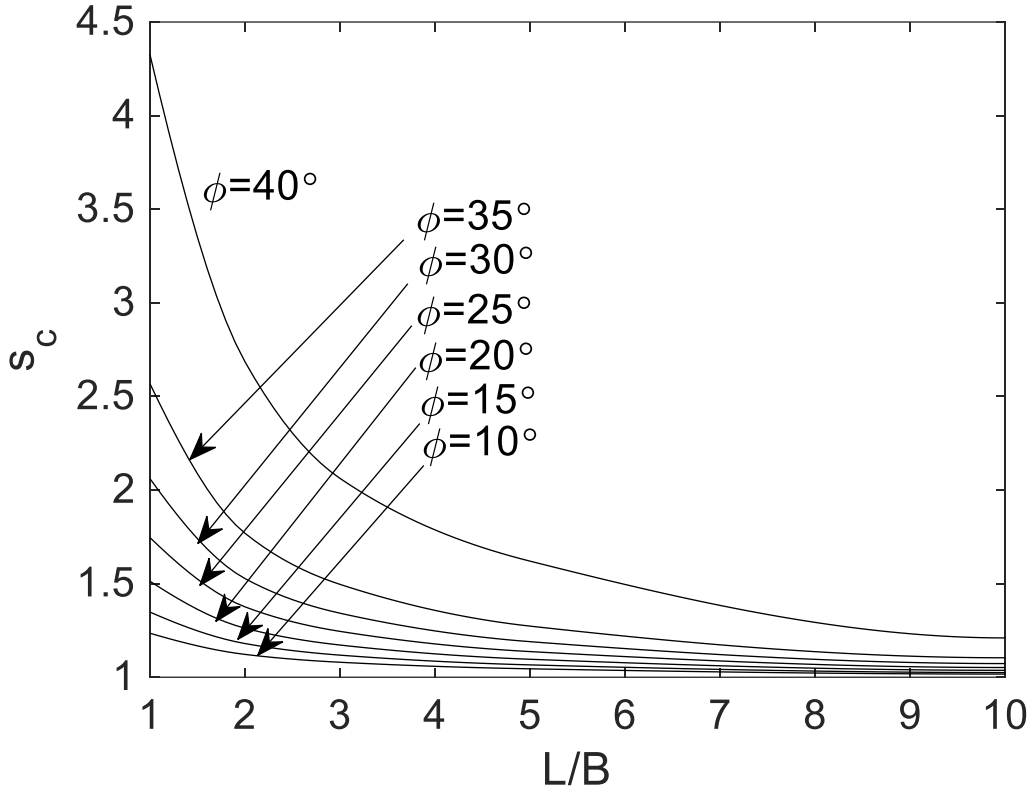

Figure 9: Values of shape factor s_c in smooth rectangular footings

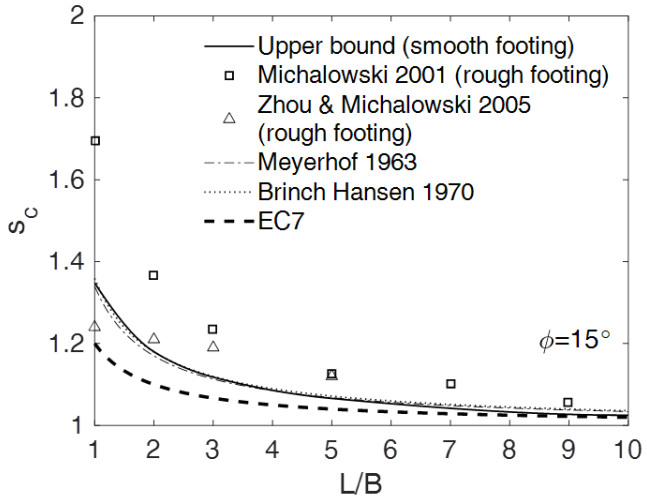

(a)

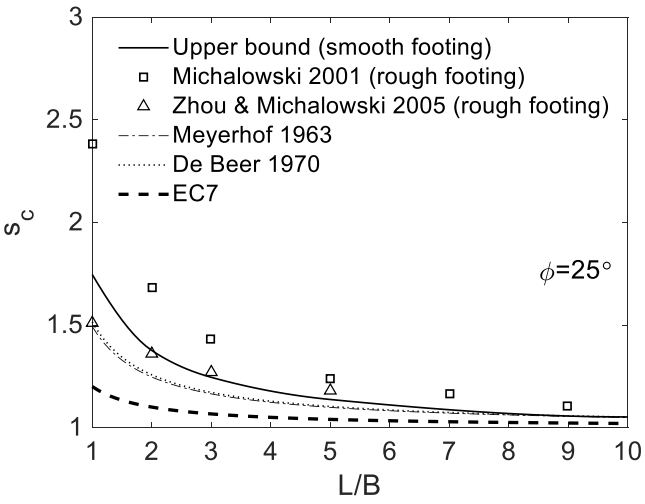

(b)

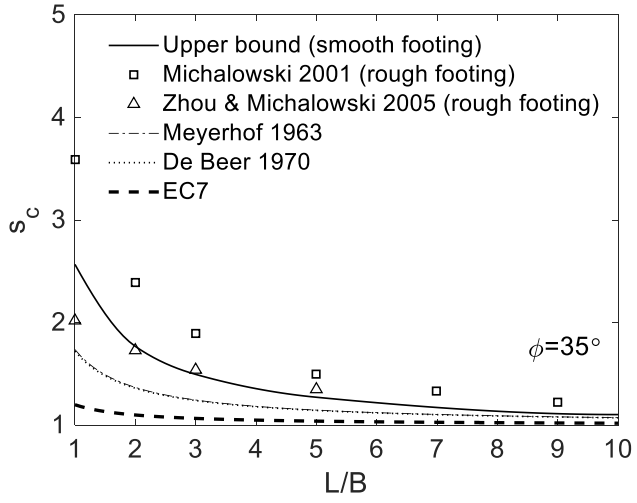

(c)

Figure 10: Values of shape factor s_c comparison with previously published results (a) ϕ =15° (b) ϕ =25° (c) ϕ =35°

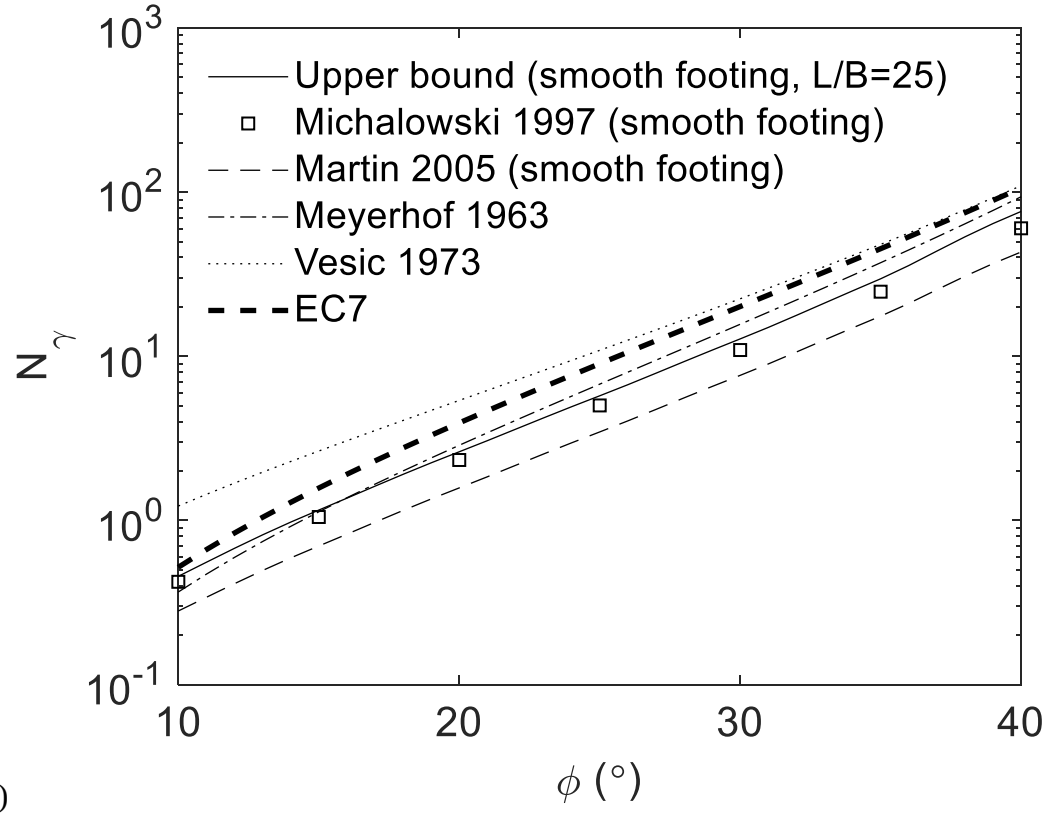

(a)

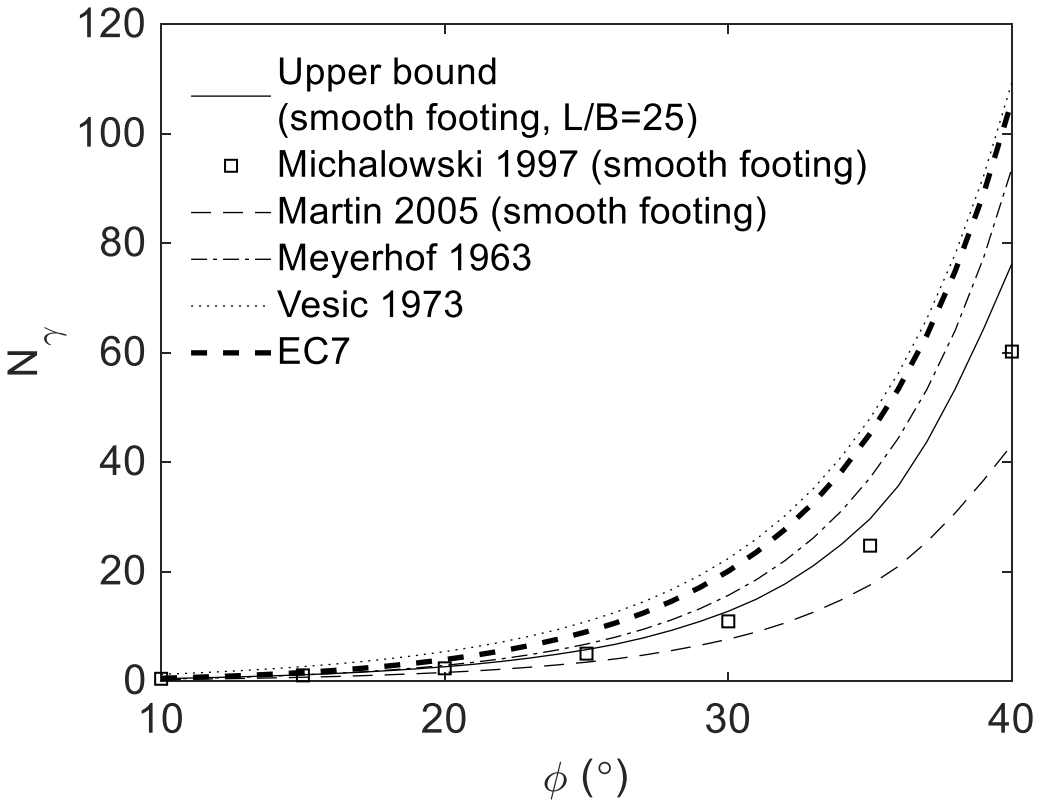

(b)

Figure 11: Bearing capacity factor N_{γ} for strip footing (a) log-linear scale (b) linear scale

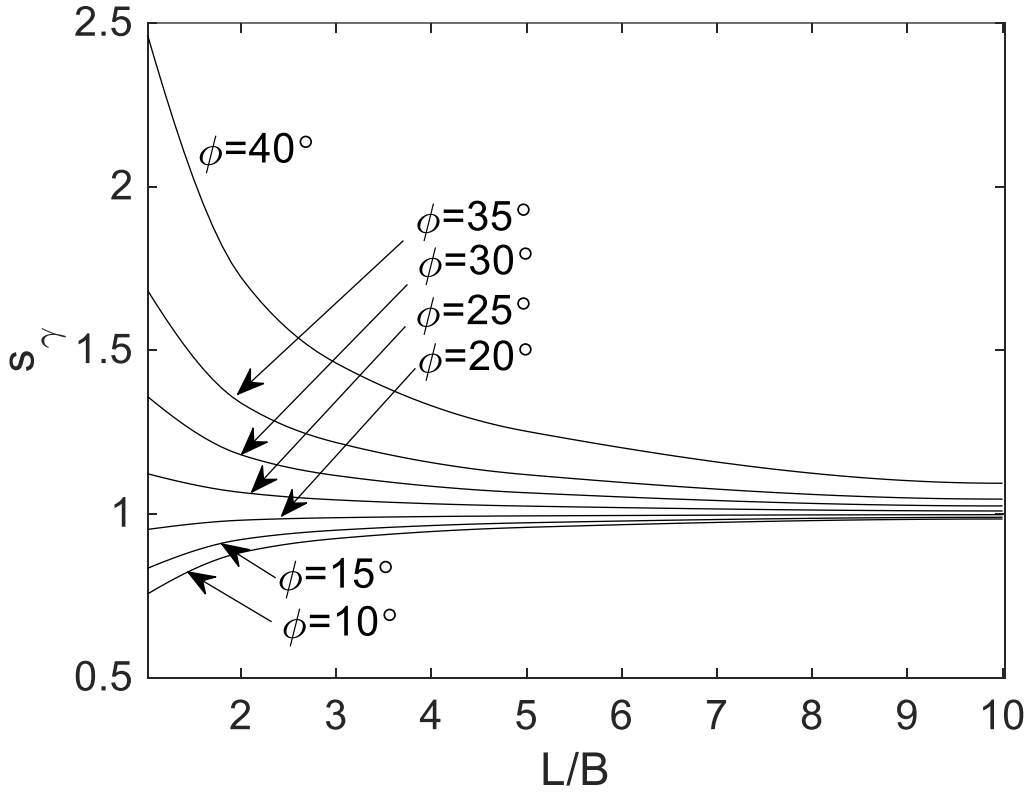

Figure 12: Values of shape factor s_γ in smooth rectangular footings

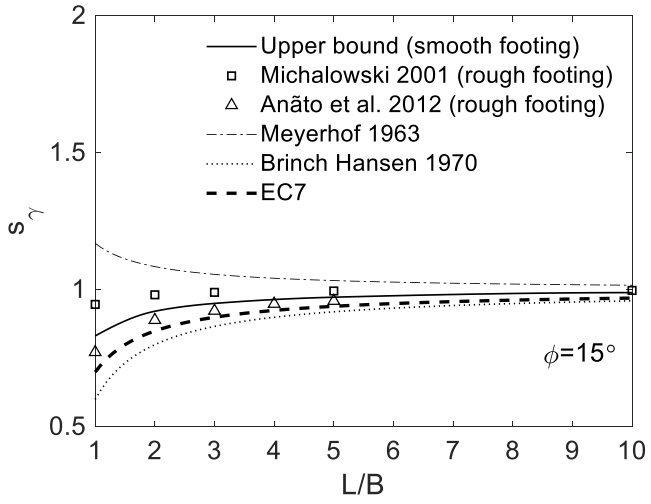

(a)

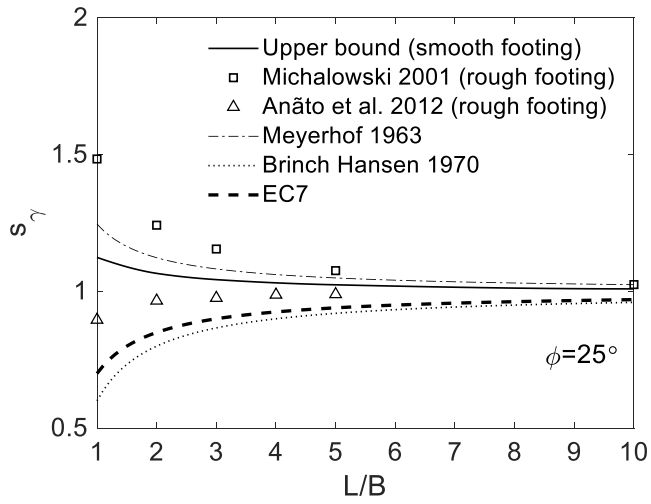

(b)

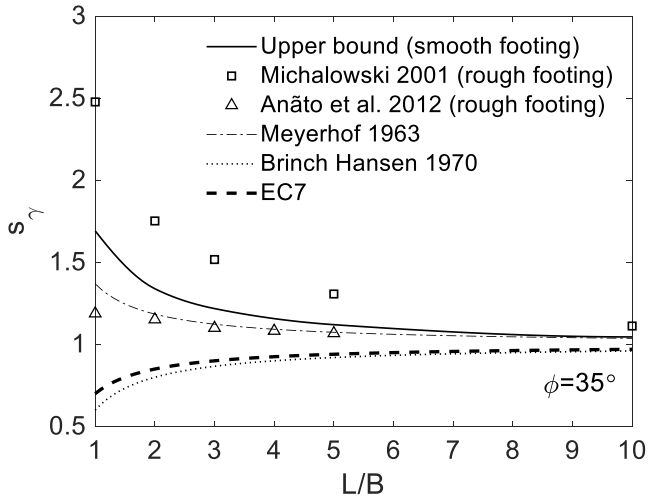

(c)

Figure 13: Values of shape factor s_γ comparison with previously published results (a) ϕ =15° (b) ϕ =25° (c) ϕ =35°